

Slow expanders invade by forming dented fronts in microbial colonies

Hyunseok Lee¹, Jeff Gore¹ and Kirill S. Korolev*²

¹Physics of Living Systems Group, Department of Physics, Massachusetts Institute of Technology, Cambridge, MA 02139

²Department of Physics, Graduate Program in Bioinformatics, Biological Design Center, Boston University, Boston, MA 02215

Abstract

Abstract:

Most organisms grow in space, whether they are viruses spreading within a host tissue or invasive species colonizing a new continent. Evolution typically selects for higher expansion rates during spatial growth, but it has been suggested that slower expanders can take over under certain conditions. Here, we report an experimental observation of such population dynamics. We demonstrate that the slower mutants win not only when the two types are intermixed at the front but also when they are spatially segregated into sectors. The latter was thought to be impossible because previous studies focused exclusively on the global competitions mediated by expansion velocities but overlooked the local competitions at sector boundaries. We developed a theory of sector geometry that accounts for both local and global competitions and describes all possible sector shapes. In particular, the theory predicted that a slower, but more competitive, mutant forms a dented V-shaped sector as it takes over the expansion front. Such sectors were indeed observed experimentally and their shapes matched up quantitatively with the theory. In simulations, we further explored several mechanism that could provide slow expanders with a local competitive advantage and showed that they are all well-described by our theory. Taken together, our results shed light on previously unexplored outcomes of spatial competition and establish a universal framework to understand evolutionary and ecological dynamics in expanding populations.

Significance

Living organisms never cease to evolve, so there is a significant interest in predicting and controlling evolution in all branches of life sciences from medicine to agriculture. The most basic question is whether a trait should increase or decrease in a given environment. The answer seems to be trivial for traits such as the growth rate in a bioreactor or the expansion rate of a tumor. Yet, it has been suggested that such traits can decrease rather than increase during evolution. Here, we report

*korolev@bu.edu

33 a mutant that outcompeted the ancestor despite having a slower expansion velocity. To explain
34 this observation, we developed and validated a theory that describes spatial competition between
35 organisms with different expansion rates and arbitrary competitive interactions.

36 Introduction

37 Population dynamics always unfold in a physical space. At small scales, microbes form tight associa-
38 tions with each other, substrates, or host cells [1, 2]. At large scales, phyto- and zooplanktons form
39 complex patterns influenced by ecological interactions [3–5] and hydrodynamics [6, 7]. Between
40 these two extremes, populations constantly shrink and expand in response to changing conditions,
41 and there is still a great deal to be learned about how spatial structure affects ecology and evolu-
42 tion [8–12]. Better understanding of these eco-evolutionary dynamics is essential for management
43 of invasive species [13, 14], controlling the growth of cancer [15], and preserving biodiversity [16,
44 17].

45 It is particularly important to understand how natural selection operates at the edge of expanding
46 populations. These expansion frontiers are hot spots of evolution because mutations that arise at
47 the edge can rapidly establish over large areas via allele surfing or sectoring [18–21]. Furthermore,
48 numerous studies argue that selection at the expansion front favors faster expanders and therefore
49 makes population control more difficult [22–32]. Indeed, organisms that expand faster have a head
50 start on growing into a new territory and may face weaker competition or better access to nutrients.
51 A well-known example is the evolution of cane toads which increased the expansion speed by 5 fold
52 over 50 years [33]. Yet, despite substantial empirical evidence across many systems [23–26, 28–32],
53 it has been suggested that the simple intuition of “faster runner wins the race” does not always
54 hold.

55 Two theoretical studies have found that slower dispersal could evolve in populations with a strong
56 Allee effect, i.e a negative growth rate at low population densities [34–36]. Slow mutants never-
57 theless can take over the populations because they are less likely to disperse ahead of the front
58 into regions with low densities and negative growth rates. In a different context, both theory and
59 experiments have shown that slow cheaters could invade the growth front of fast cooperators [27,
60 37]. In this system, the production of public goods allowed cooperators to expand faster, but made
61 them vulnerable to the invasion by cheaters.

62 The examples above show that slower expanders succeed in the presence of a tradeoff between local
63 and global fitness. The global fitness is simply the expansion rate of a given species in isolation,
64 which determines how quickly it can colonize an empty territory. When two species are well-
65 separated in space, their competition is determined solely by the global fitness. In contrast, when
66 the two species are present at the same location, their competition could involve differences in
67 growth rates, production of public goods [38, 39], or secretion of toxins [40]. We refer to such local
68 competitive abilities as local fitness. It is natural to assume that slow expanders can win only if
69 they are superior local competitors, but it is not clear a priori if this is actually feasible or how to
70 integrate local and global fitness under various scenarios of spatial competition.

71 Our interest in the interplay between local and global competition was sparked by an unusual

72 spatial pattern in colonies of *Raoutella planticola* grown on agar plates. These colonies repeatedly
73 developed depressions or dents along the edge. We found that dents were produced by a spontaneous
74 mutant that expanded slower than the wildtype. Thus, we discovered a convenient platform to
75 explore the fate of slower expanders in spatial competition and to elucidate the tension between
76 local and global fitness.

77 In our experiment, the slower expander took over the colony either by increasing in frequency
78 homogeneously along the front or by forming pure, mutant-only, sectors. When mutant sectors
79 formed, they had an unusual “dented” or “V” shape. To explain this spatial pattern, we developed a
80 theory that describes all possible sector geometries. Our theory unifies local and global competitions
81 without assuming any particular mechanism for growth and dispersal. Although mechanism-free,
82 the theory makes quantitative predictions, which we confirmed experimentally. We also simulated
83 multiple mechanistic models to demonstrate that the takeover by slower expanders is generic and
84 could occur due to multiple ecological mechanisms. These simulations further confirmed that sector
85 shape prediction from geometric theory is universal. Taken together, our results establish a new
86 framework to understand evolutionary and ecological dynamics in expanding populations with
87 arbitrary frequency- and density-dependent selection.

88 Results

89 *Experimental observation of slow mutants taking over the front*

90 The strains used in our experiment were derived from a soil isolate of *Raoultella planticola*, a Gram-
91 negative, facultatively anaerobic, non-motile bacterium that is found in soil and water and can
92 occasionally lead to infections [41, 42]. We grew *R. planticola* on a hard LB agar plate (1.5% agar)
93 and noticed the formation of V-shaped dents along the front. Such dents were reproducibly observed
94 in biological replicates (Fig. S1). Suspecting that dents were caused by a mutation, we isolated
95 cells from the smooth parts of the colony edge (wildtype) and from the dents (mutant) (Fig. 1A).

96 We first characterized the expansion dynamics of the two strains in isolation by inoculating each
97 culture at the center of a hard agar plate. Both strains formed smooth, round colonies, which
98 expanded at a constant velocity (Fig. 1B, Fig. S2). The wildtype had about 50% larger expansion
99 velocity compared to the mutant. Thus, the evolved strain was a slower expander.

100 Our observations seemed paradoxical given numerous observations of invasion acceleration due to
101 genetic changes that increase expansion velocities [33, 43]. However, range expansions are known to
102 produce high genetic drift [44, 45] and, therefore, allow for the fixation of deleterious mutations [20,
103 46–49]. So, we next investigated whether the mutant has a selective advantage in competition with
104 the wildtype within the same colony.

105 We competed the two strains by inoculating an agar plate with a drop containing a 99:1 mixture
106 of the wildtype and the mutant. We used two wildtype strains (and their respective mutants) with
107 different fluorescent labels and the spatial patterns were analyzed with fluorescence microscopy
108 (see Methods). After about 48 hours of growth, a ring of mutant completely encircled the wild-
109 type (Fig. 1C). Only the mutant ring continued to expand, while the expansion of the wildtype

110 ceased (Fig. S3). Thus the mutant not only localized to the front but also achieved a greater pop-
111 ulation size. This is quite different from other microbial systems where a strain with poor motility
112 localized to the front without suppressing the growth of faster strain and without producing a
113 larger biomass [50, 51]. Thus, our experiments strongly suggest that the mutant has a competitive
114 advantage despite its lower expansion velocity.

115 *Experimental observation of slow mutants invading by forming dented fronts*

116 Our initial competition experiments did not exhibit the dents that sparked our initial interest in
117 the strains. The mutant took over uniformly across the expansion front, producing a rotationally
118 invariant spatial pattern (Fig. 1C). In fact, one might even argue that the success of the mutant
119 could have been entirely due to the transient growth dynamics, and the wildtype would prevail if
120 allowed to somehow spatially segregate from the mutant. To address both of these concerns, we
121 sought to alter the experiments so that the mutant and the wildtype grow as distinct sectors within
122 the same colony.

123 In microbial colonies, sectors emerge due to genetic drift at the growing edge. The magnitude
124 of demographic fluctuations varies widely in different systems, depending on the organism, the
125 growth conditions, and the duration of the experiment [52, 53]. To test for the effects of sectoring,
126 we needed to increase stochasticity without altering other aspects of the competition. Reducing
127 the cell density of the initial inoculant accomplished this goal. By lowering the inoculant density
128 (from 10^{-1} OD₆₀₀ to 10^{-3} OD₆₀₀), we increased the separation between cells that localized to the
129 colony edge following the drying of the inoculation drop. This in turn dramatically increased the
130 formation of monoclonal sectors (Fig. 1D).

131 Although sectoring spatially segregated the two strains and, thus, allowed the wildtype to expand
132 with a higher velocity, the slower mutant still outcompeted the wildtype (Fig. 1D, Fig. 1E). The
133 takeover of mutant was robust under different choices of initial density, initial mutant fraction, and
134 fluorescent label (Fig. S4, Fig. S5). The takeover by the mutant also produced the characteristic
135 V-shaped dents at the colony edge. These dents are the exact opposite of the bulges or protrusions
136 that one usually observes for beneficial mutations [54]. Typically, the advantageous mutants have
137 a greater expansion velocity and, therefore, outgrow the ancestors at the front. For our strains,
138 however, the winning mutant had a lower expansion velocity, and this lower expansion velocity
139 produced the opposite of the bulge—the dent.

140 *Mechanism-free theory of sector geometry*

141 Our experiments unambiguously demonstrated that a slower expander can indeed outcompete a
142 faster expander with and without sectoring. Still, we need a careful theoretical description of the
143 spatial dynamics to reconcile the apparent contradiction between the slow global expansion of the
144 mutant and its superior performance in local competition. We could approach this question by
145 simulating a specific ecological mechanism that could be responsible for the tradeoff between local
146 and global fitness. However, it is much more useful to first ask what can be said about spatial
147 competition generically and determine the range of possible sector shapes without relying on any

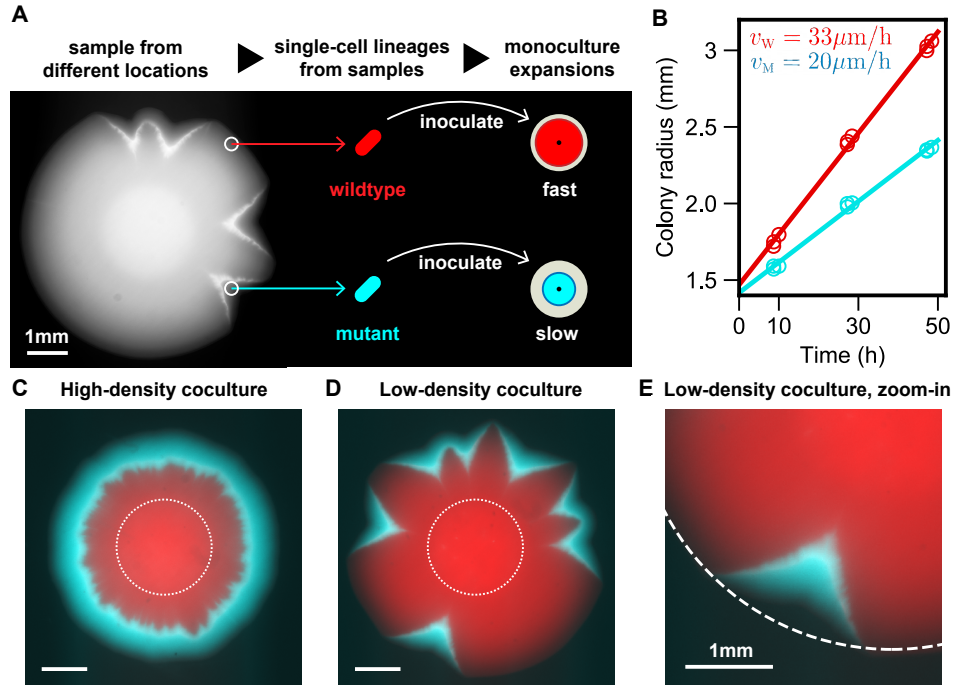


Figure 1: Slow mutant takes over the front with and without sector formation. (A) We found that wildtype *R. planticola* colonies develop V-shaped indentations; a bright-field image is shown. We sampled cells from the dents and non-dented regions and then developed strains descending from a single cell (see Methods). (B) The mutant expanded more slowly than the wildtype. The data points come from two technical replicates, and the line is a fit. (C, D) Despite its slower expansion, the mutant wins in coculture. Fluorescence images show the spatial patterns 48 hours after inoculation with a 99:1 mixture of the wildtype and mutant. A ring of mutant (cyan) outran and encircled wildtype (red) when the mixed inoculant had a high density (OD_{600} of 10^{-1}). Mutant sectors emerged and widened over the front when the mixed inoculant had a low density (OD_{600} of 10^{-3}). Images are taken 48 hours after inoculation, and dotted lines represent initial inoculant droplets. (E) A zoomed image of a V-shaped sector (from the bottom of D). Dotted circle is a fit from wildtype expansion. The advantage of the mutant and its slower expansion is evident from the lateral expansion of the cyan sector.

148 specific mechanism.

149 All possible sector shapes can be determined from simple geometric considerations (Fig. 2A, SI Ap-
150 pendix) that rely on a few standard assumptions. The expansion velocities of the two strains (v_W
151 and v_M) are assumed to be time-independent both to simplify the calculations and to reflect ex-
152 perimental observation (Fig. 1B). We also assume, consistent with past studies [55–57], that there
153 is little growth behind the front so that the spatial pattern remains once established as in our
154 experiments. Finally, we neglect long-range interactions due to the diffusion of nutrients, toxins, or
155 signalling molecules¹ [58–60]. The outcome of the local competition between the strains then are
156 captured by a single parameter: the velocity u with which the mutant invades laterally into the
157 population of the wildtype.

158 The knowledge of the three velocities (v_W , v_M , and u) is sufficient to simulate how the shape of the
159 colony changes with time. In some situations, colony shapes can also be obtained analytically by
160 comparing the position of the front at two times t and $t + \Delta t$. We derive the equations for sector
161 shapes by requiring that all distances between the corresponding points of the two fronts are given
162 by Δt times the appropriate velocity (Fig. 2A). The details of these calculations are provided in
163 the SI (Fig. S8).

164 We found that all possible sector shapes fall into three classes. Without loss of generality, we take u
165 to be positive by calling the mutant the strain that invades locally. The shape of the sector is then
166 largely determined by v_M/v_W . When this ratio is less than one, sectors have a dented shape. In
167 the opposite case, sectors bulge outwards. The exact shape of the front of course depends on all
168 three velocities. Overall, there are the two broad classes discussed above and a special limiting case
169 when $u = \sqrt{v_M^2 - v_W^2}$ which is discussed below. In all cases, we obtained sector shapes analytically
170 for both circular and flat initial fronts (SI Fig. S9, Fig. S10). The latter are summarized in Fig. 2B
171 and are used to test the theoretical predictions.

172 The geometrical theory provides a concrete way to define local fitness advantage, u/v_W , and global
173 fitness advantage, $v_M/v_W - 1$. These two types of fitness can take arbitrary values, even with
174 opposite signs. The only condition is that a positive u needs to be larger than $\sqrt{v_M^2 - v_W^2}$ when the
175 mutant is faster than the wildtype. This constraint arises because, for large v_M/v_W , the gaining of
176 new territory due to the large global fitness advantage outpaces the gain in the new territory due
177 to a smaller local fitness advantage. The constraint on u is not relevant to dented fronts, so we
178 relegate this discussion to the SI (Fig. S7).

179 *Experimental test of the geometric theory*

180 How can we test whether the theory of sector geometry described above indeed applies to our
181 experiments? The theory utilizes three velocities v_W , v_M , and u to predict the shape of the sector
182 boundary and the sector front. The absolute values of the velocities determine how quickly the
183 colony grows overall and its shape depends only on two dimensionless parameters: v_M/v_W and u/v_W .
184 The first parameter can be obtained from the direct measurements of expansion velocities in mono-

¹The addition of long-range interactions would provide greater modelling flexibility and therefore make it easier to observe novel spatial patterns such as a V-shaped sector. Our works shows that this extra flexibility is unnecessary and dented fronts can appear in purely local models.

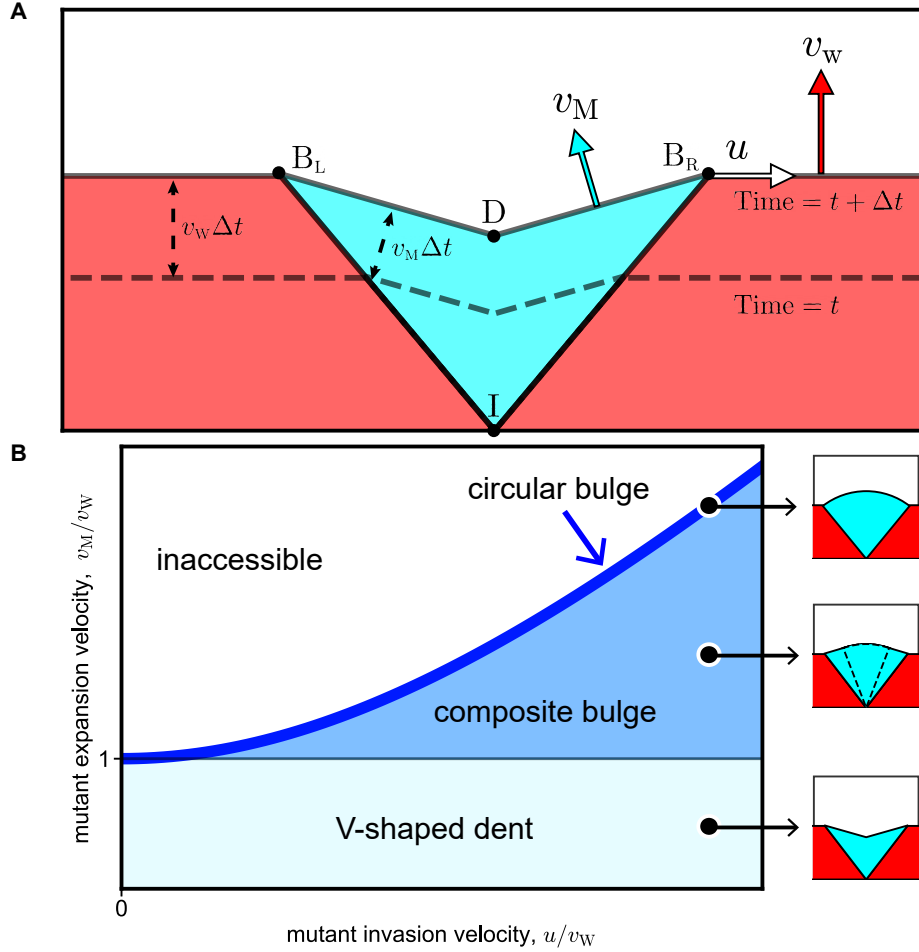


Figure 2: Geometric theory predicts sector shapes as a function of local and global fitness. Flat-front initial conditions are illustrated here, and the corresponding results for circular fronts are shown in the SI. (A) The shape of the mutant sector can be derived from geometric considerations. During a time interval Δt , the boundary points B_L and B_R move upward by $v_W\Delta t$ and laterally outward by $u\Delta t$. The position of the dent D is obtained from the requirement that both $\overline{DB_L}$ and $\overline{DB_R}$ shift by $v_M\Delta t$; the directions of the shifts are perpendicular to $\overline{DB_L}$ and $\overline{DB_R}$ respectively. Point I labels the origin of the sector. (B) The geometric theory predicts sector shapes as a function of u/v_W and v_M/v_W . When $v_M < v_W$ and $u > 0$, the mutant forms a V-shaped dented front; note that all boundaries are straight lines. When $v_M > v_W$ and $u > \sqrt{v_M^2 - v_W^2}$, the mutant forms a bulged front. The shape of the bulge consists of two regions. It is an arc of a circle near the middle and two straight lines near the two boundaries between the mutant and the wildtype. The circular region grows and the linear region shrinks as v_M/v_W increases at constant u/v_W . The bulge becomes completely circular when v_M/v_W reaches its maximal value of $\sqrt{1 + u^2/v_W^2}$ on the boundary of the accessible region. See SI for derivation and exact mathematical expressions of all sector shapes.

185 cultures. The second parameter can be inferred by fitting the shape of the sector boundary to
 186 the theory. This leaves the shape of the sector front as an independent measurement that can be
 187 compared to the theoretical prediction.

188 The linear expansion geometry greatly simplifies all the steps involved in testing the theory be-
 189 cause the shapes of both the sector boundary and the dent are determined by their opening angles.
 190 Qualitative agreement with this theoretical prediction is quite clear from the experimental im-
 191 ages (Fig. 3A), which indeed show that mutant sectors are bounded by straight lines on all sides.
 192 The opening angle of the sector boundary determines u/v_W and the opening angle of the dent serves
 193 as a testable prediction (Fig. 3B).

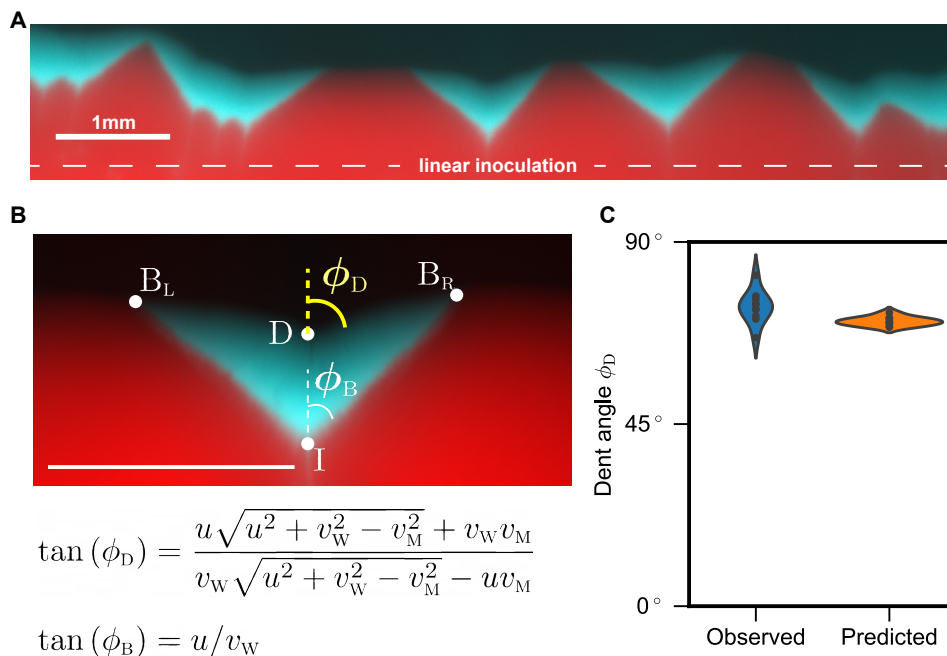


Figure 3: Empirical test of predicted sector shapes. (A) We used linear inoculations with low density and low fraction of the mutant and grew the colonies for 48 hours. (B) Top: Zoom-in image of one of the sectors. The shape of mutant sector is quantified by two opening angles: one between the two sector boundaries $2\phi_B$ and one between the two parts of the expansion front that meet at the dent $2\phi_D$. Bottom: The theory predicts ϕ_B and ϕ_D as functions of the three velocities: v_W , v_M , and u . We used ϕ_B to determine u/v_W and predict ϕ_D ; v_M/v_W is measured from monoculture expansions. (C) The observed and predicted values of ϕ_D are very close to each other.

194 Our experiments proceeded as follows. We first measured expansion velocities in monocultures by
 195 tracking the colony radius as a function of time; see Fig. 1B. Then, the data on sector shapes were
 196 collected from plates inoculated along a straight line with a low-density (10^{-3} OD₆₀₀) 99:1 mixture
 197 of the wildtype and the mutant. After two days of growth, five well-isolated sectors were analyzed to
 198 determine ϕ_B and ϕ_D (see Methods). Since each side of the angle can be used, we effectively obtained
 199 ten measurements. Figure 3C shows that observed ϕ_D is 73.93° (SD=3.81°, SEM=1.21°, n=10).
 200 Predicted ϕ_D is 70.39° (SD=1.02°, SEM=0.32°, n=10). This is an excellent agreement given other
 201 sources of variability in our experiment including variations in velocity between replicates and
 202 potential systematic errors in fitting sector shapes. Thus the geometric theory not only provides

203 an explanation of the novel sector shape, but also describes it quantitatively.

204 *Concrete mechanisms of fitness tradeoff*

205 The geometric theory integrates local and global competition and quantitatively predicts the shape
206 of mutant sector in our experiment. Yet, the theory does not provide a tangible mechanism behind
207 the takeover by a slower expander. To show that dented fronts emerge readily under different
208 ecological scenarios we used the flexible framework of reaction-diffusion models, which are also
209 known as generalized Fisher-Kolmogorov equations [61–63]. A general model can be written as:

$$\begin{aligned}\partial_t n_W &= (\nabla^2 (D_W n_W) + r_W n_W) (1 - n_W - n_M), \\ \partial_t n_M &= (\nabla^2 (D_M n_M) + r_M n_M) (1 - n_W - n_M).\end{aligned}\tag{1}$$

210 Here, n_W and n_M are the population densities of the wildtype and the mutant normalized by the
211 shared carrying capacity; D_W , r_W and D_M , r_M are their respective dispersal and per capita growth
212 rates. The shared carrying capacity ensures that there is no growth behind the front [54].

213 The simplest model takes all four parameters to be density-independent constants. It is then easy
214 to show that there is no difference between local and global fitness; see Fig. S6 and Ref. [54]. Most
215 of the previous work focused on this special case of so-called “pulled” waves [64] and thus could
216 not observe the takeover by the slower expander.

217 Many organisms, however, exhibit some density dependence in their growth or dispersal dynam-
218 ics [65–69], which can lead to a tradeoff between local and global fitness. One commonly-studied
219 case is found in the interaction between cooperators and cheaters [27, 50, 70, 71]. To model this
220 ecological scenario, we take

$$\begin{aligned}D_W &= D_M = D, \\ r_W &= r \left(1 - \alpha \frac{n_M}{n_W + n_M} \right), \quad r_M = r \left(1 - s + \alpha \frac{n_W}{n_W + n_M} \right).\end{aligned}\tag{2}$$

221 The benefit of cooperation is specified by s , which is the difference in the growth rate of cooperators
222 and cheaters when grown in isolation. The benefit of cheating is controlled by α ; the growth rate of
223 cheaters increases by up to α provided cooperators are locally abundant. For simplicity, we chose
224 a symmetric linear dependence of the growth rates on the mutant frequency and assumed that the
225 diffusion constants are equal.

226 Numerical simulations of this model reproduced a V-shaped dented front (Fig. 4A). The dents
227 flattened when there was no benefit to cooperate ($s = 0$) and were replaced by bulges when
228 cooperators grew slower than cheaters ($s < 0$). We were also able to test whether these transitions
229 in sector shape matched the predictions of the geometric theory. For this comparison between the
230 theory and simulations, we need a mapping between the microscopic parameters of the model and
231 the three velocities that enter our geometric theory. Fortunately, in this model, all three velocities

232 can be calculated analytically: $v_W = 2\sqrt{rD(1+s)}$, $v_M = 2\sqrt{rD}$, and $u = \sqrt{(\alpha-s)rD}$. Therefore,
 233 we could overlay individual simulations on the phase diagram predicted by the geometric theory.
 234 The result, shown in Fig. 4A, shows the expected agreement and provides further validation for the
 235 geometric theory.

236 The geometric description is generic and should transcend the specifics of the cooperator-cheater
 237 model discussed above. To further illustrate that different ecological interactions can produce
 238 identical spatial patterns, we simulated a completely different mechanism for the tradeoff between
 239 local and global fitness. This time, we assumed that the wildtype loses the local competition
 240 because it grows slower than the mutant, but this slower growth is more than compensated by a
 241 much higher dispersal rate. This growth-dispersal tradeoff may be common in nature [29, 72–74],
 242 and is captured by the following set of parameters:

$$\begin{aligned}
 D_W = D_M = D_0 - D_1 \frac{n_M}{n_W + n_M}, \\
 r_W = r, \quad r_M = r(1+s).
 \end{aligned}
 \tag{3}$$

243 Here, the growth rates are density-independent, but the dispersal rates change with the local
 244 community composition. We chose $D_W = D_M$ both for analytical tractability and to reflect the
 245 collective nature of movement in colonies of non-motile microbes [75, 76], which are pushed outward
 246 by mechanical stress generated within the colony.

247 Our simulations again exhibited dented fronts and all shape transitions in full agreement with the
 248 geometric model (Fig. 4B). Thus, the geometric description is universal, i.e. a wide set of growth-
 249 dispersal dynamics converges to it. This universality, however, makes it impossible to determine
 250 the specifics of ecological interactions from spatial patterns alone. In other words, the observation
 251 of a dented front indicates the existence of a tradeoff between local and global fitness, but does not
 252 hint at any specific mechanism that is responsible for this tradeoff.

253 Discussion

254 This study used a simple and well-controlled laboratory microcosm to elucidate the factors that
 255 influence spatial competition. We found a stark contradiction to the intuitive expectation that the
 256 faster runner wins the race [32]. A mutant that expanded more slowly on its own nevertheless took
 257 over the expansion front when inoculated with the wildtype. This spatial takeover accompanied
 258 V-shaped sectors, which are a characteristic signature of the mismatch between local and global
 259 competition. To explain these observations, we developed a theory that integrates local and global
 260 competition and predicts all possible sector shapes. We then confirmed the validity of the theory
 261 using both further experiments and simulations.

262 Our experimental results unequivocally demonstrate that a slow expander can win with and without
 263 sectoring. Under low genetic drift conditions, the slow expander took over the front uniformly across
 264 the colony. This outcome can be described by one-dimensional models because the competition
 265 occurs primarily along the radial direction. In contrast, stronger genetic drift resulted in sector

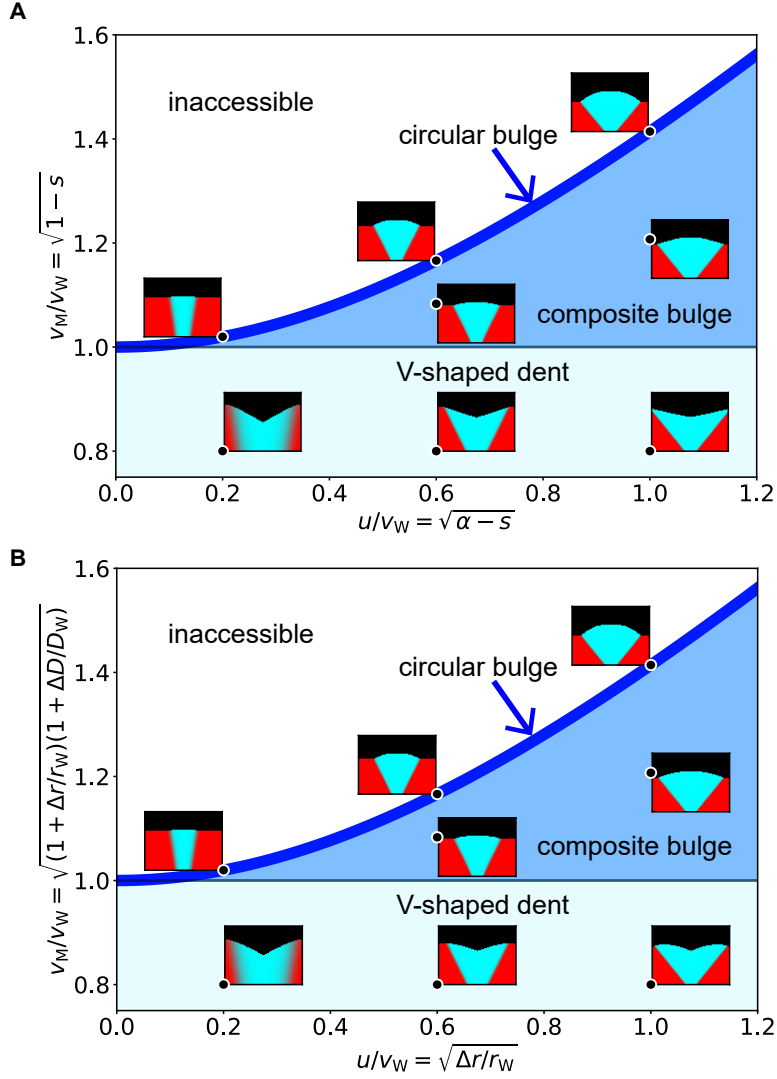


Figure 4: Sector shapes from microscopic simulations recapitulate phase diagram from the geometric theory. (A) Simulation of cooperor-cheater model (Eq. 2) is compared with the geometric theory. By varying s (benefit from cooperation) and α (strength of cheating), we explored sector shapes for different values of v_M/v_W and u/v_W . The locations of various sector shapes match the predictions of the geometric theory. In particular, V-shaped dents are observed when a cheater expands more slowly than a cooperor ($s > 0$), but has a sufficiently large advantage from cheating ($\alpha > s$). (B) Simulations of growth-dispersal tradeoff model (Eq. 3) also agree with the geometric theory. Different sector shapes were obtained by varying the the growth advantage s and and the dispersal disadvantage D_1 . See Methods for simulation parameters.

266 formation and produced fully two-dimensional growth dynamics. Even under these less favorable
267 conditions, the slower mutant still outcompeted the wildtype.

268 Previously, slower expanders were found to be successful only in one-dimensional models [34, 36,
269 37], and only bulged sectors of faster expanders were reported for two-dimensional growth [54].
270 The latter was true even when there was a tradeoff between local and global fitness [77], presumably
271 because local fitness advantage was not sufficiently large. Our experiments not only confirm the
272 predictions of one-dimensional models, but also expand the set of conditions under which the
273 unusual takeover by a slower mutant can be observed. In fact, the slower expanders could be
274 successful in many settings not only because the theory and simulations strongly support this
275 claim, but also because we relied on evolved mutants from natural isolates rather than genetic
276 engineering to obtain the strains.

277 The observation of dented fronts clearly shows that the existing theoretical understanding of sector
278 growth is incomplete. Previously, it was assumed that the spatial pattern depends only on the
279 ratio of the mutant and wildtype velocities [54]. This simple picture holds when the fast expander
280 also has a moderate advantage in local competition. More generally, however, we found that the
281 outcome of the competition also depends on the velocity u with which one of the strains invades
282 locally. The sector shapes are completely determined by the three velocities (v_M, v_W, u) and can be
283 used to make quantitative inferences from experimental data. Nevertheless, the main contribution
284 of our theory is its ability to integrate local and global competition and predict how large scale
285 spatial patterns emerge from species interactions.

286 The geometric theory is not without limitations. This phenomenological theory cannot predict
287 whether the fast or the slow mutant wins in a given system. To answer that question, one needs
288 to consider a mechanistic model and derive how the invasion velocity u depends on microscopic
289 parameters, which we have done for specific models. The universal nature of the geometric theory
290 also precluded us from identifying the mechanism responsible for the growth dynamics observed in
291 our experiments. We left this fascinating question for future works, and instead, focused on several
292 common tradeoffs between local and global fitness. The simulations of these tradeoffs not only
293 confirmed the validity of the geometric theory, but further highlighted that slower expanders could
294 establish by a wide range of mechanisms.

295 The geometric theory also relies on a few technical assumptions such as constant expansion ve-
296 locities, negligible stochasticity, and the absence of long-range interaction due to chemotaxis or
297 nutrient depletion. Relaxing these assumptions could lead to certain quantitative changes in sector
298 shapes, but the existence of dented fronts or the possibility of a takeover by a slower expander
299 should not be affected.

300 Our work opens many directions for further investigation. We clearly showed that the expansion
301 velocity cannot be the sole determinant of the spatial competition. Therefore, it will be important to
302 examine how local interactions influence the eco-evolutionary dynamics during range expansions.
303 Such future work would bring about a more detailed description of ecological and biophysical
304 processes in growing populations. It would also greatly enhance our understanding of the tradeoffs
305 among different life-history traits and shed light on the incredible diversity of successful strategies
306 to navigate spatial environments [29, 72–74]. The geometric theory developed here provides a
307 convenient way to integrate these various aspects of population dynamics. It abstracts the main
308 features of spatial growth and should facilitate the analysis of both experiments and simulations.

309 Material and Method

310 *Strains*

311 Wildtype *Raoultella planticola* strains were isolated from a soil sample (MIT Killian Court, Cam-
312 bridge, MA) [78] and were tagged with two different fluorescent proteins mScarlet-I (red) and
313 mTurquoise2 (cyan) by insertion of plasmids pMRE145 and pMRE141 respectively [79]. As we grew
314 wildtype colonies on agar plates, they reproducibly developed dents after several days as shown in
315 Fig. 1A and Fig. S1. We sampled the cells from either inside the dent or on the smooth edge using
316 inoculation loops, streaked on small plates, and grown in 30°C for two days. Then we sampled
317 single colonies, grew them overnight in LB growth media, and stored as a -80°C glycerol stock.

318 *Growth media preparation*

319 We prepared hard agar plates with 1X Luria-Bertani media (LB, 2.5% w/v; BD Biosciences-US)
320 and 1.5% w/v of agar (BD Bioscience-US). We also added 1X Chloramphenicol (Cm, 15mg/L,
321 prepared from 1000X solution) for constitutive expression of fluorescence. For each agar plate,
322 4mL of media was pipetted into a petri dish (60X15mm, sterile, with vents; Greiner Bio-one), and
323 was cooled overnight (15 hours) before inoculation.

324 *Expansion experiment*

325 For each strain, -80°C glycerol stock was streaked on a separate plate and grown for 2 days. Then
326 a colony from each strain was picked up and put into a 50mL Falcon Tube filled with 5 mL of
327 liquid media (1X LB and 1X Cm). Bacterial cultures were grown overnight at 30°C under constant
328 shaking 1350 rpm (on Titramax shakers; Heidolph). We then diluted and mixed the cultures to
329 desired total density and mutant fraction, measured in optical density (OD₆₀₀) using a Varioskan
330 Flash (Thermo Fisher Scientific) plate reader. For circular expansions, we gently placed a droplet
331 of 1.5 μ L inoculant at the center of an agar plate. For linear expansions, we dipped a long edge of
332 a sterile cover glass (24X50mm; VWR) gently into the culture and touched the agar plate with the
333 edge. After inoculation, each colony was grown at 30°C for 48 hours.

334 *Imaging*

335 At fixed times after inoculation, each plate was put on a stage of Nikon Eclipse Ti inverted light
336 microscope system. 10X magnification was used for whole-colony images, and 40X magnification
337 was used for single sector images. Fluorescent images were taken using Chroma filter sets ET-
338 dsRed (49005) and ET-CFP (49001) and a Pixis 1024 CCD camera.

339 We used scikit-image [80] for image processing in Python. Images from different fluorescent chan-
340 nels were integrated after background subtraction and normalization by respective maximum in-
341 tensity. The sector boundaries were identified as the furthest points from inoculation plane where

342 both strains' FL intensities were above respective thresholds. The codes for image analysis will
343 be available via GitHub (https://github.com/lachesis2520/dented_front_public.git) upon
344 publication.

345 *Numerical simulation*

346 Numerical simulations were performed by solving the corresponding partial differential equations
347 on a square grid using a forward-in-time finite difference scheme that is second order accurate in
348 space and first order accurate in time [81]. Python codes will be available via GitHub (https://github.com/lachesis2520/dented_front_public.git) upon publication.
349 For cooperator-cheater model simulation, we used the following set of values for parameters (s, α) :
350 $(-0.04, 0)$, $(-0.36, 0)$, $(-1, 0)$, $(-0.173, 0.187)$, $(-0.457, 0.543)$, $(0.36, 0.4)$, $(0.36, 0.72)$, and $(0.36, 1.36)$.
351 For growth-dispersal tradeoff model simulation, we used (s, D_1) of $(0.04, 0)$, $(0.36, 0)$, $(1, 0)$, $(0.36, 0.147)$,
352 $(1, 0.271)$, $(0.04, 0.385)$, $(0.36, 0.529)$, and $(1, 0.68)$.
353

354 **Acknowledgements**

355 We thank all members of the J.G. laboratory for helpful discussions. Anthony Ortiz provided the
356 wildtype *R. planticola* strain and Daniel R. Amor helped with preliminary work for this study.
357 This work was supported by NIH (R01-GM102311) to J.G. and by the Simons Foundation Grant
358 #409704, Cottrell Scholar Award #24010, and by NIGMS grant #1R01GM138530-01 to K.S.K.
359 The authors also acknowledge the MIT SuperCloud and Lincoln Laboratory Supercomputing Center
360 for providing computational resources.

361 Supplemental Information

362 **Contents**

363	I. Supplementary figures	16
364	II. Geometric theory and sector shapes	22
365	Introduction	22
366	Linear inoculation	24
367	Circular inoculation	27

368 I. Supplementary figures

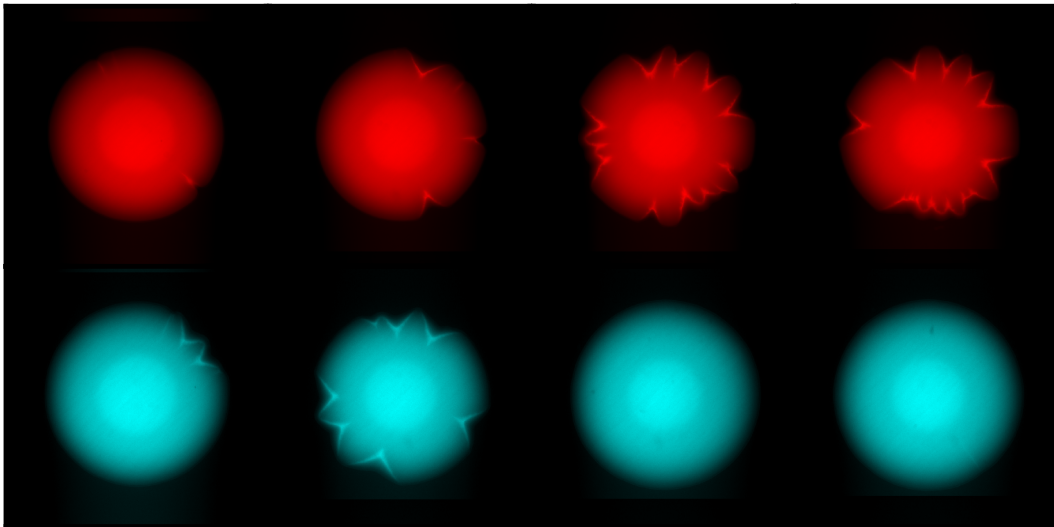


Figure S1: Emergence of dents in wildtype colonies was reproducible. Wildtype colonies were grown for 48 hours. Top: wildtype strains constitutively expressing mScarlet-I. Bottom: wildtype strains constitutively expressing mTurquoise-2.

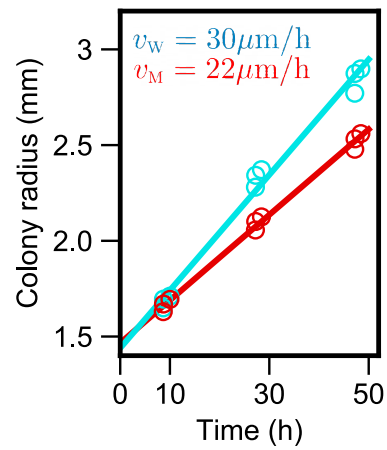


Figure S2: Mutant expands more slowly regardless of the choice of fluorescent labels. Wildtype with mTurquoise-2 fluorescence protein expanded with $v_W = 30 \mu\text{m}/\text{h}$ while mutant with mScarlet-I fluorescence protein expanded with $v_M = 22 \mu\text{m}/\text{h}$.

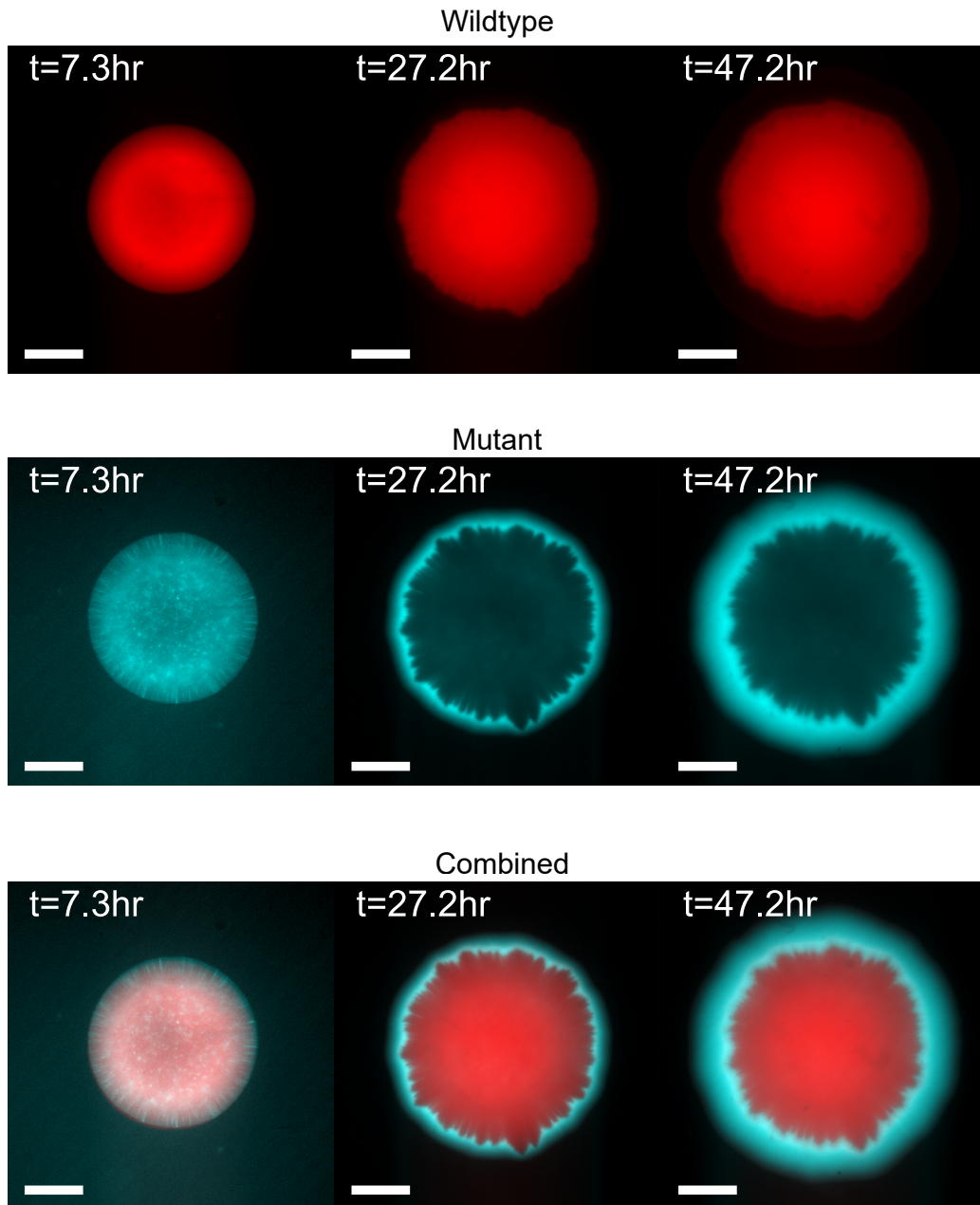


Figure S3: In co-culture experiment, wildtype did not expand after a day while mutant kept expanding. Top: Fluorescence images of wildtype cells during expansion. Middle: Fluorescence images of mutant cells during expansion. Bottom: combined.

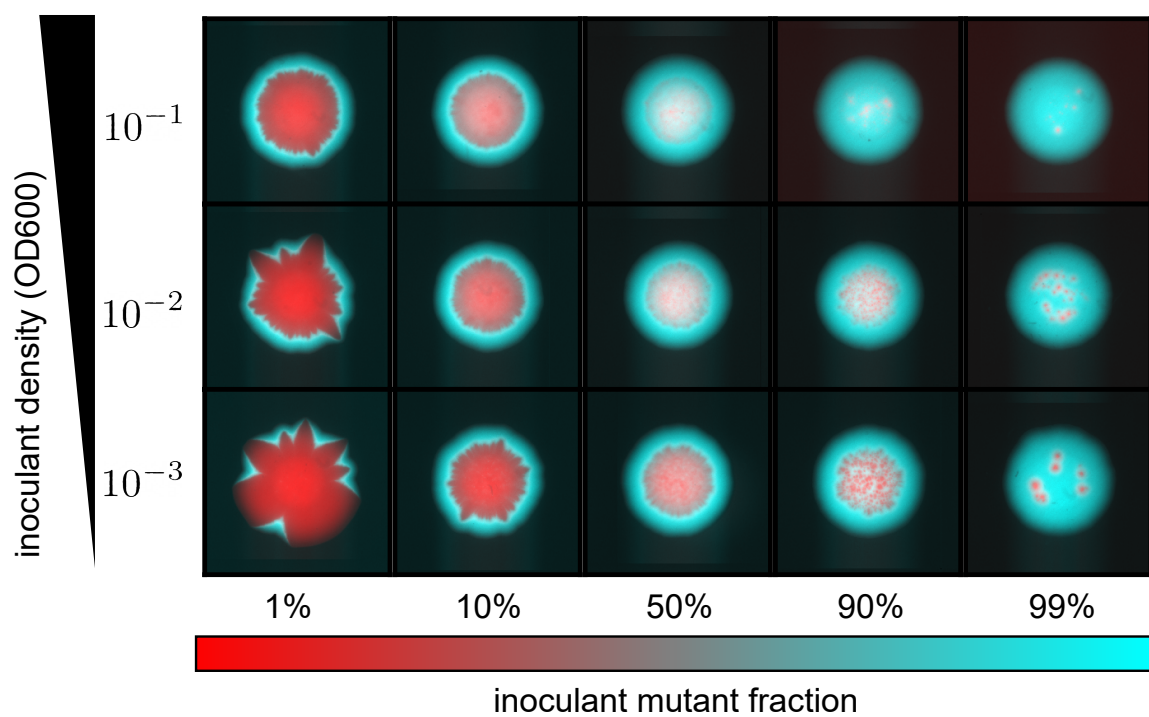


Figure S4: Mutant outcompetes wildtype under a wide range of inoculant densities and initial mutant fractions.

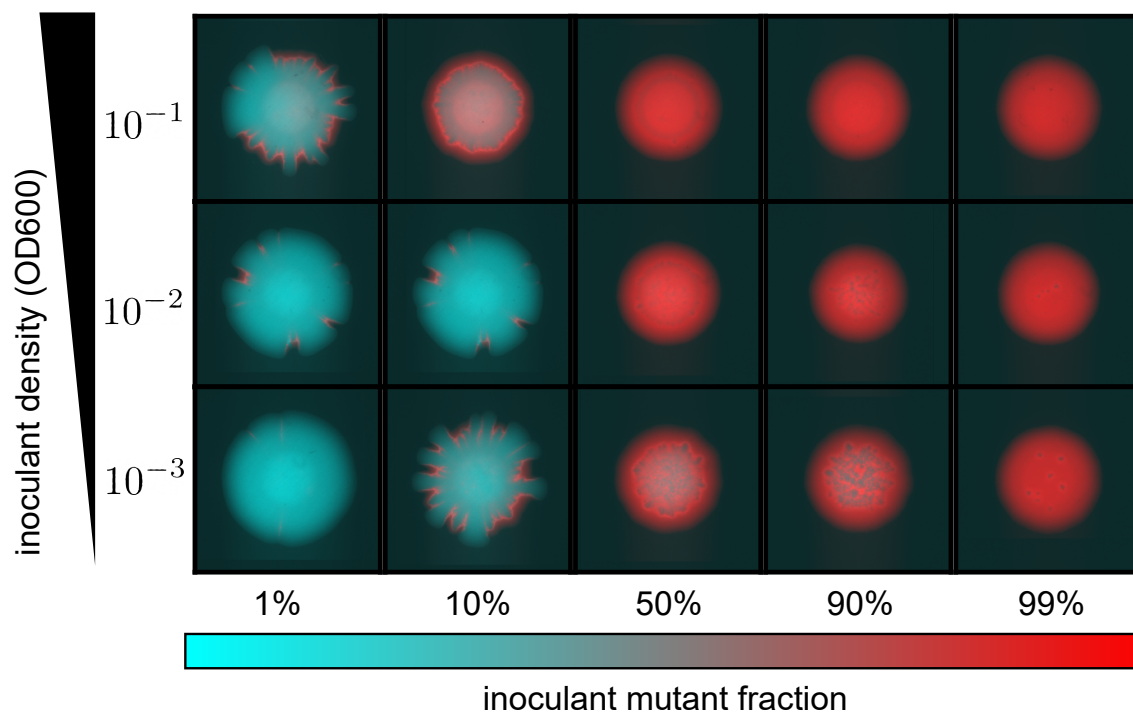


Figure S5: Mutant outcompetes wildtype under a different choice of fluorescent labels of wildtype and mutant.

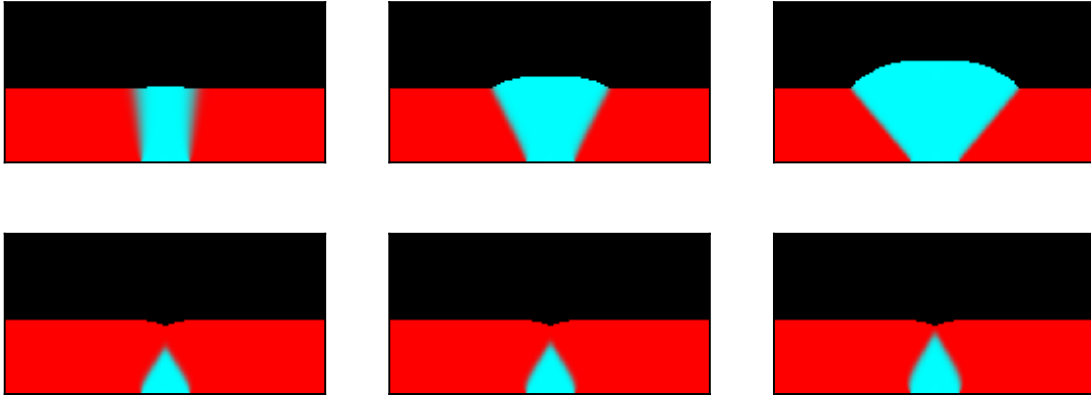


Figure S6: No dented fronts occur in simulations with density-independent growth and dispersal. In each column, the growth advantage $r_M/r_W - 1$ is the same (Left: 0.04, Middle: 0.36, Right:1). Simulations in top row have $D_W = D_M$, so that the ratio of the expansion velocities varies with the growth rates ($v_M = v_W \sqrt{r_M/r_W}$). For the bottom row, we used $D_M = \frac{0.64r_W}{r_M} D_W$ so that $v_M = 0.8v_W$. We observed no expanding mutant sectors when its expansion velocity was less than that of the wildtype.

369 II. Geometric theory and sector shapes

370 *Introduction*

371 During spatial growth in microbial colonies or other cellular aggregates, mutants appear and com-
 372 pete with each other. Previous studies [54] and common intuition suggest that advantageous
 373 mutants should form a sector that bulges out of the expansion front. In the main text, we reported
 374 experiments showing that this is not always the case. Here, we identify all possible shapes that can
 375 result from competition between two types in a growing colony.

376 To make progress, we make a number of approximations and work in the so-called geometrical
 377 optics limit. This limit assumes that the expansion front and the boundary between the types
 378 can be treated as thin lines. Neglecting sector and boundary widths is justified when these length
 379 scales are much smaller than the colony size. In small colonies, thin boundaries require strong
 380 genetic drift and slow motility. Furthermore, we assume that the expansion velocity of each type
 381 remains fixed. In particular, we neglect the effects of spatial variation in nutrient concentration
 382 due to protrusions of one type ahead of the other. This approximation is valid for high nutrient
 383 concentrations and when the size of the protrusions is small compared to the size of the mutant
 384 sector.

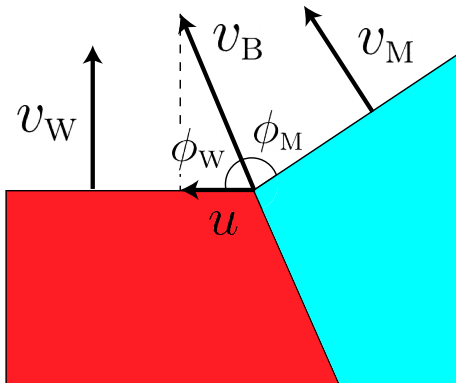


Figure S7: Geometry of the competition.

385 In the geometric-optics limit, the competition between two types is described by three velocities:
 386 the velocity of mutant v_M , the velocity of wildtype v_W , and the velocity of the boundary v_B , which
 387 are shown in Fig. S7. (Note $v_B \neq u$) Previous work [54] focused on the regime when v_B was
 388 determined by v_M and v_W ; in contrast, we make no assumptions about the relative magnitude of
 389 these three velocities.

390 In the close vicinity of the sector boundary, the two expansion fronts can be approximated as
 391 straight lines. Their position (Fig. S7) is determined by requiring that the expansion along the
 392 boundary with velocity v_B results in the same displacement of the fronts as moving perpendicular
 393 to them with velocities v_M and v_W respectively:

$$v_W = v_B \sin \phi_W, \tag{S1}$$

$$v_M = v_B \sin \phi_M. \tag{S2}$$

394 For linear inoculations, the above equations are sufficient to completely specify sector shapes be-
 395 cause, as we show below, the expansion fronts are straight lines even away from the sector boundary.
 396 For circular initial conditions, Eqs. (S2) provide information only about the local orientation at
 397 the sector boundary, and further calculations are necessary. One way to obtain global shape is to
 398 write down partial differential equations that specify how the position of the front changes and use
 399 Eqs. (S2) as the boundary conditions. A much simpler approach is to use an equal time argument
 400 from Ref. [54].

401 This method traces the ancestral lineage from each point along the front and requires that the time
 402 traveled on that lineage is equal to the current time t . The location of the ancestral lineage is such
 403 that it takes the shortest time to reach the initial population starting from a given point without
 404 entering the space occupied by the other type. The details of these calculations are provided below.

405 Before proceeding, we note that, here and in the main text, we typically parameterize the problem
 406 with velocity u rather than v_B . Since u is defined as the velocity of the boundary point along the
 407 front of wildtype, we can obtain it by projecting the boundary velocity on the expansion front of
 408 the wildtype:

$$u = v_B \cos \phi_W. \tag{S3}$$

409 From this equation and Eq. (S2), it follows that

$$v_B = \sqrt{v_W^2 + u^2}. \tag{S4}$$

410 In the following, we assume that mutant takes over the front, i.e. $u > 0$. Mutants with negative u
 411 immediately become extinct at least in the deterministic model considered here.

412 Finally, we observe that Eqs. (S2) impose constraints on the values of the three velocities. In
 413 particular, since sines are always less than one, the boundary velocity v_B must be greater or equal
 414 than both v_M and v_W . In terms of u , this implies that

$$v_M \leq \sqrt{u^2 + v_W^2}. \tag{S5}$$

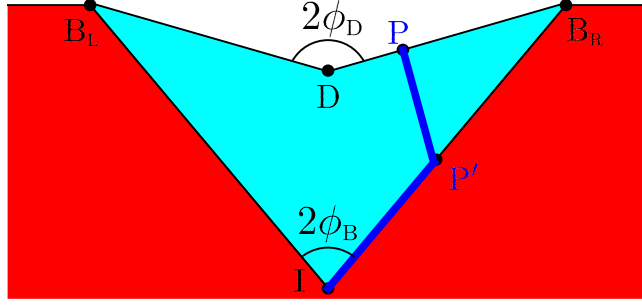


Figure S8: Sector shape for linear inoculation and $v_M < v_W$. Sectors of faster wildtype (red) and slower mutant (cyan) meet at sector boundary \overline{IB}_L and \overline{IB}_R . It takes the shortest time for the mutant to go from its initial location at I to a point on the front P by first following $\overline{IP'}$ and then $\overline{P'P}$ (blue path). The resulting geometry can be characterized by two opening angles: $2\phi_B$ for the sector boundary and $2\phi_D$ for the expansion front.

415 *Linear inoculation*

416 **Sector boundary**

417 Linear expansion geometry, the simplest situation to consider, allows us to explain the essence of
 418 the equal time argument. This geometry is illustrated in Fig. S8. Initially ($t = 0$), the colony front
 419 is located at $y = 0$, and expansion proceeds in the upper half-plane. Mutant is only present at a
 420 single point, which we put at $x = 0$; the rest of the front is occupied by the wildtype.

421 As the expansion proceeds, the region near $x = 0$ is affected by the competition between the types.
 422 From the definition of u , the extent of this region is given by $x \in (-ut, ut)$. Regions further away
 423 are however unaffected and expand as if only wildtype is present. Thus, for $|x| \geq ut$, the front is
 424 located at $y = v_W t$. From these considerations, we can further conclude that the sector boundary
 425 is described by $(ut, v_W t)$. Note that, below, we consider only the right side of the expansion; the
 426 left side is described by the mirror image with respect to the y -axis. Thus,

$$\tan \phi_B = \frac{u}{v_W}. \quad (\text{S6})$$

427 Note that, $\phi_B = \phi_W - \pi/2$, which is clear from Figs. S7 and S8.

428 The shape of the front for $|x| < ut$ depends on the relative values of v_M , v_W , and u .

429 $v_m \leq v_w$

430 When mutant is slower than wildtype, we find that front has a V-shaped dent with an opening
 431 angle $2\phi_D$ as shown in Fig. S8. To derive this result, we take a point P on the front with yet
 432 unknown coordinates (x_p, y_p) . Note that $x_p \in (0, ut)$. Then, we should obtain the location of the
 433 ancestral lineage that connects this point to the initial location of the mutant: point I . Because
 434 the ancestral lineage is located so that to minimize the travel time, it must be a union of straight
 435 lines. Indeed, it is a well-known fact from geometrical optics that light rays travel on straight
 436 lines except where the value of the refraction index changes [82]. In our case, this means that the
 437 ancestral lineages of mutant can consist of straight lines within the mutant sector and regions of
 438 the boundary. Obviously, the ancestral lineage of the mutant cannot penetrate the region occupied
 439 by the wildtype.

440 The equal time argument then offers us two possibilities: a direct connection \overline{IP} and an indirect
 441 connection $\widehat{IP'P}$ via a point P' on the sector boundary. The times to traverse these paths are

$$T_{PI} = |PI|/v_M, \quad (S7)$$

$$T_{PP'I} = |PP'|/v_M + |P'I|/v_B. \quad (S8)$$

442 To complete the analysis, we need to choose the path with the lowest travel time and determine all
 443 locations of P for which the travel time equals t . For the direct connection, it is clear that P must
 444 lie on an arc of a circle with the radius of $v_M t$ centered at I . For the indirect connection, we first
 445 need to determine the location of P' , which must minimize the travel time.

446 Since P' lies on the sector boundary its coordinates are given by $(ut', v_w t')$ with an unknown t' .
 447 The travel time is then given by

$$T_{PP'I} = \frac{\sqrt{(x_p - ut')^2 + (y_p - v_w t')^2}}{v_M} + \frac{\sqrt{u^2 + v_w^2} t'}{v_b}. \quad (S9)$$

448 Upon minimizing $T_{PP'I}$ with respect to t' , we find that

$$t' = \frac{u\sqrt{u^2 + v_w^2 - v_M^2} + v_M v_w}{(u^2 + v_w^2)\sqrt{u^2 + v_w^2 - v_M^2}} \left(x_p + \frac{u v_w - v_M \sqrt{u^2 + v_w^2 - v_M^2}}{u^2 - v_M^2} y_p \right), \quad (S10)$$

449 and the travel time equals

$$T_{PP'I} = \frac{(u v_M - v_w \sqrt{u^2 + v_w^2 - v_M^2}) x_p + (v_M v_w + u \sqrt{u^2 + v_w^2 - v_M^2}) y_p}{(u^2 + v_w^2) v_M}, \quad (S11)$$

450 which is smaller than T_{PI} as long as $v_M < v_W$. Thus, the ancestral lineages takes an indirect path
 451 that first connects point P to the sector boundary and then follows the sector boundary until I .
 452 The shape of the front is determined by setting $T_{PP'I}$ from Eq. (S11) equal to t . This results in a
 453 segment of a straight line, and a straightforward calculation shows that

$$\phi_D = \arctan \left(\frac{u\sqrt{v_W^2 + u^2 - v_M^2} + v_M v_W}{v_W \sqrt{v_W^2 + u^2 - v_M^2} - u v_M} \right). \quad (\text{S12})$$

454 Because the front and the sector boundaries are straight, the result above also directly follows from
 455 Eqs. (S7). Indeed, a simple geometric argument shows that $\phi_D = \phi_M + \phi_W - \pi/2$.

456 Note that, for $v_M = v_W$, the angle $\phi_D = \pi/2$ and the whole front is flat as it should if the expansion
 457 rates of the strains are identical.

$$458 \quad v_{\mathbf{m}} = \sqrt{v_W^2 + u^2}$$

459 In the limiting case of maximal allowed v_M , the shape of the sector is also simple and immediately
 460 follows from the calculations above. Now, as we compare the two alternative paths, we find that T_{PI}
 461 is always smaller than $T_{PP'I}$. Thus, the shape of the sector is an arc of a circle of radius $v_M t$ around I
 462 that connects to the flat front of the wild type at the sector boundary.

463 Previous work that used the equal time argument to describe competition in microbial colonies
 464 only considered $v_M = \sqrt{v_W^2 + u^2}$ and missed other possible front shapes [54]. While it might appear
 465 that $v_M = \sqrt{v_W^2 + u^2}$ is a very special case, this relationship between the velocities holds across a
 466 wide set of conditions. Specifically, $v_M = \sqrt{v_W^2 + u^2}$ whenever local competition between the types
 467 is not strong enough to alter the priority effects due to different expansion velocities.

$$468 \quad v_W < v_{\mathbf{m}} < \sqrt{v_W^2 + u^2}$$

469 The remaining possibility is the hybrid of the two cases considered so far. Depending on how far P
 470 is from the sector boundary, the quickest path from P to I may be either the direct or the indirect
 471 connection. We find that the front around $x = 0$ is a semicircle of radius $v_M t$, but it is a straight
 472 line near the sector boundaries. The two segments joint smoothly. The angular half-width of the
 473 central arc, $\phi_{\text{transition}}$, and the slope of the linear segment (see Fig. S9) are given by

$$\phi_{\text{transition}} = \arctan \left(\frac{u v_M - v_W \sqrt{v_W^2 + u^2 - v_M^2}}{v_M v_W + u \sqrt{v_W^2 + u^2 - v_M^2}} \right), \quad (\text{S13})$$

$$\text{slope} = - \frac{u v_M - v_W \sqrt{v_W^2 + u^2 - v_M^2}}{v_M v_W + u \sqrt{v_W^2 + u^2 - v_M^2}}. \quad (\text{S14})$$

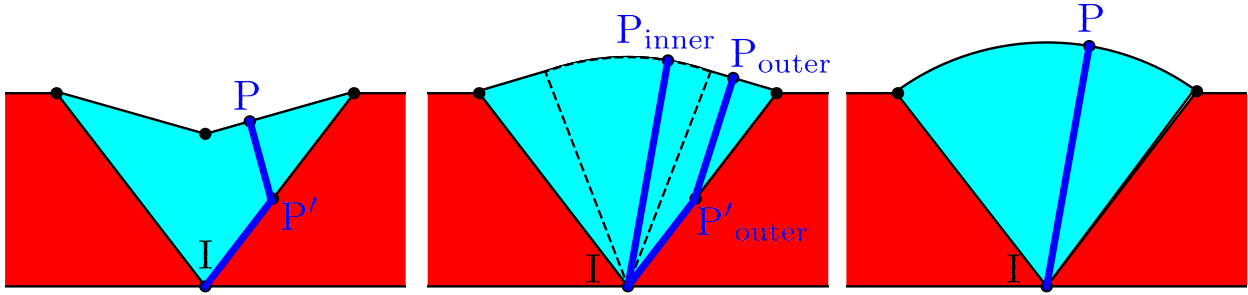


Figure S9: Possible sector shapes for linear inoculation. Left: $v_M < v_W$. The mutant sector emerging from point I has a dented front. The front consists of two straight lines. The shortest-time path follows the sector boundary and also enters the sector interior. Middle: $v_W < v_M < \sqrt{v_W^2 + u^2}$. The mutant sector is a composite bulge. The front consists of two straight lines and an arc. To reach a point P_{outer} on straight part of the expansion front, the shortest-time path first follows the sector boundary before entering the sector interior. To reach a point P_{inner} on the arc, the shortest-time path follows a straight line from I to P_{inner} . Right: $v_M > \sqrt{v_W^2 + u^2}$. The front is an arc. To reach a point P on the front, the shortest-time path follows a straight line from I to P .

474 *Circular inoculation*

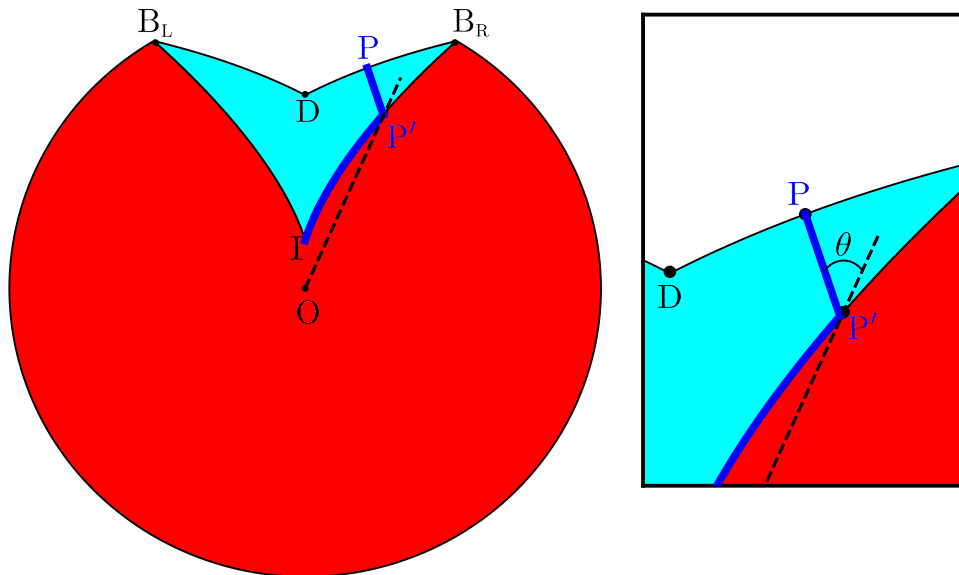


Figure S10: Circular colony with a dented front, $v_W > v_M$. The path of the shortest time follows the sector boundary from I to P' and then a straight line connecting P' and P . Note that $\overline{P'P}$ and $\overline{OP'}$ always intersect at angle θ .

475 We assume that the expansion starts at $t = 0$ when wildtype colony fills the circle with radius
 476 $r \leq r_0$, and the mutant is present only at $I = (r_0, 0)$ in polar coordinates.
 477

478 Sector boundary

479 The boundary between the mutant and the wild type moves with linear velocity u along the front. In
 480 polar coordinates, the position of the sector boundary (r_B, ϕ_B) then obeys the following equation

$$\frac{d\phi_B}{dt} = \frac{u}{r_B}. \quad (\text{S15})$$

481 We can eliminate time by using $dr_B/dt = v_W$ to obtain

$$\phi_B(r_B) = \frac{u}{v_W} \ln\left(\frac{r_B}{r_0}\right). \quad (\text{S16})$$

482 We also find that the length of boundary at time t is $\sqrt{v_W^2 + u^2}t$, and thus

$$v_B = \sqrt{v_W^2 + u^2} \quad (\text{S17})$$

483 just as in the linear case.

$$484 \quad v_m < v_w$$

485 Let us consider a point $P = (r_p, \phi_p)$ on a mutant patch with $\phi_p > 0$ for simplicity.

486 As described before, we first find $T_{PP'I}$ by minimizing $\frac{|PP'|}{v_M} + \frac{|P'I|}{v_W}$ over points P' on the sector
 487 boundary. The point $P' = (r_{P'}, \phi_{P'})$ should satisfy two equations:

$$488 \quad \phi_{P'}(r_{P'}) = \frac{u}{v_W} \ln\left(\frac{r_{P'}}{r_0}\right), \quad (\text{S18})$$

$$489 \quad \frac{d}{dr_{P'}} \left(\frac{r_{P'} - r_0}{v_W} + \frac{\sqrt{(r_p \cos \phi_p - r_{P'} \cos \phi_{P'})^2 + (r_p \sin \phi_{P'} - r_{P'} \sin \phi_p)^2}}{v_M} \right) = 0. \quad (\text{S19})$$

490 Here, the first equation constrains P' to be on the sector boundary, and the second equation
 491 minimizes $T_{PP'I}$ over P' . Since there are two unknowns and two equations, we can solve for
 492 $(r_{P'}, \phi_{P'})$. The solution is conveniently written in an implicit form:

$$\begin{aligned} \frac{r_{P'} \sin \phi_{P'} - r_p \sin \phi_p}{r_{P'} \cos \phi_{P'} - r_p \cos \phi_p} &= -\tan(\theta - \phi_{P'}), \\ \theta &= \arctan \left(\frac{uv_M - v_W \sqrt{v_W^2 + u^2 - v_M^2}}{v_M v_W + u \sqrt{v_W^2 + u^2 - v_M^2}} \right). \end{aligned} \quad (\text{S20})$$

493 This tells that $\overline{PP'}$ is parallel to $(1, \theta - \phi_{P'})$; the angle between $\overline{PP'}$ and $\overline{P'O}$ is a constant θ
 494 independent of r_p, ϕ_p . Note that $\theta > 0$ for $v_M < v_W$, and thereby every point P on mutant front

495 with ϕ_p has its corresponding P' on sector boundary \widehat{IB} .

496

497 The next step toward identifying the front position at time T is to find all points P such that
 498 $T_{PP'I} = T$. Using the mapping between P and P' described above, we find P by first moving along
 499 sector boundary and then moving in a straight line parallel to $(1, \theta - \phi_{P'})$. By varying the time
 500 t' spent along the sector boundary while keeping the total time T fixed, we obtain a parametric
 501 expression for $P(T) = (x_p(T), y_p(T))$ in Cartesian coordinates:

$$\begin{aligned} x_p(T; t') &= (v_w t' + r_0) \sin\left(\frac{u}{v_w} \ln\left(\frac{r_0 + v_w t'}{r_0}\right)\right) + v_M(T - t') \sin\left(\frac{u}{v_w} \ln\left(\frac{r_0 + v_w t'}{r_0}\right) - \theta\right), \\ y_p(T; t') &= (v_w t' + r_0) \cos\left(\frac{u}{v_w} \ln\left(\frac{r_0 + v_w t'}{r_0}\right)\right) + v_M(T - t') \cos\left(\frac{u}{v_w} \ln\left(\frac{r_0 + v_w t'}{r_0}\right) - \theta\right). \end{aligned} \quad (\text{S21})$$

502 It is also possible to get a non-parametric, explicit expression by solving an equivalent partial
 503 differential equation using the method of characteristics:

$$\begin{aligned} \phi_p(t, r) &= \frac{u}{v_w} \ln\left(1 + \frac{v_w t}{r_0}\right) + F\left(\frac{r}{r_0 + v_w t}\right) - F(1), \quad \text{where} \\ F(\rho) &= \frac{u}{2v_w} \ln\left(\frac{(\rho^2 v_w^2 - v_M^2) \sqrt{\rho^2 - \frac{v_M^2}{v_w^2 + u^2}} - \frac{uv_M}{v_w \sqrt{v_w^2 + u^2}}}{\sqrt{\rho^2 - \frac{v_M^2}{v_w^2 + u^2}} + \frac{uv_M}{v_w \sqrt{v_w^2 + u^2}}}\right) \\ &+ \arctan\left(\frac{\sqrt{v_w^2 + u^2}}{v_M} \sqrt{\rho^2 - \frac{v_M^2}{v_w^2 + u^2}}\right). \end{aligned} \quad (\text{S22})$$

504 $v_M > v_w$

505 In this regime, $\theta < 0$ and thereby some points P on the mutant front do not have a corresponding
 506 P' on the sector boundary. In other words, the straight path \overline{IP} takes the shortest time. We find
 507 that, when P is near the top of the bulge, the minimal path is a straight line \overline{IP} while, When P is
 508 further from the top, the minimal path is a straight line $\overline{P'P}$ followed by a curved path $\widehat{IP'}$ along
 509 the sector boundary.

510 Note that the straight path is tilted by a fixed angle θ from $\overline{OP'}$, pointing inwards to the cen-
 511 ter of the sector compared to the tangent line except when $v_M = \sqrt{v_w^2 + u^2}$. In the latter case,
 512 $\theta = -\arctan\left(\sqrt{\frac{v_M^2}{v_w^2} - 1}\right)$, and the straight path is tangent to the sector boundary, as described
 513 in [54].

514

515 The boundary between the two regions of the front lies angle $\phi_{\text{transition}}$ way from the center. This
 516 angle is given by

$$\phi_{\text{transition}} = \arctan\left(\frac{uv_M - v_w \sqrt{v_w^2 + u^2 - v_M^2}}{v_M v_w + u \sqrt{v_w^2 + u^2 - v_M^2}}\right). \quad (\text{S23})$$

517 Thus, the bulge is an arc of a circle near the center and is described by Eq. (S21) near the sector
518 boundary.

References

- 519 1. Grossart, H.-P., Kjørboe, T., Tang, K. & Ploug, H. Bacterial colonization of particles: growth
520 and interactions. *Applied and environmental microbiology* **69**, 3500–3509 (2003).
- 521 2. Datta, M. S., Sliwerska, E., Gore, J., Polz, M. F. & Cordero, O. X. Microbial interactions
522 lead to rapid micro-scale successions on model marine particles. *Nature communications* **7**,
523 1–7 (2016).
- 524 3. Durrett, R. & Levin, S. Spatial aspects of interspecific competition. *Theoretical population*
525 *biology* **53**, 30–43 (1998).
- 526 4. Ben-Jacob, E., Cohen, I. & Levine, H. Cooperative self-organization of microorganisms. *Ad-*
527 *vances in Physics* **49**, 395–554 (2000).
- 528 5. Lima-Mendez, G. *et al.* Determinants of community structure in the global plankton interac-
529 tome. *Science* **348** (2015).
- 530 6. Abraham, E. R. The generation of plankton patchiness by turbulent stirring. *Nature* **391**,
531 577–580 (1998).
- 532 7. Pigolotti, S., Benzi, R., Jensen, M. H. & Nelson, D. R. Population genetics in compressible
533 flows. *Physical review letters* **108**, 128102 (2012).
- 534 8. Skellam, J. G. Random dispersal in theoretical populations. *Biometrika* **38**, 196–218 (1951).
- 535 9. Levin, S. A. Dispersion and population interactions. *The American Naturalist* **108**, 207–228
536 (1974).
- 537 10. Hanski, I. Metapopulation dynamics. *Nature* **396**, 41–49 (1998).
- 538 11. Lin, Y. T., Kim, H. & Doering, C. R. Demographic stochasticity and evolution of dispersion
539 I. Spatially homogeneous environments. *Journal of mathematical biology* **70**, 647–678 (2015).
- 540 12. Nadell, C. D., Drescher, K. & Foster, K. R. Spatial structure, cooperation and competition in
541 biofilms. *Nature Reviews Microbiology* **14**, 589–600 (2016).
- 542 13. Mooney, H. A. & Cleland, E. E. The evolutionary impact of invasive species. *Proceedings of*
543 *the National Academy of Sciences* **98**, 5446–5451 (2001).
- 544 14. Sakai, A. K. *et al.* The population biology of invasive species. *Annual review of ecology and*
545 *systematics* **32**, 305–332 (2001).
- 546 15. Korolev, K. S., Xavier, J. B. & Gore, J. Turning ecology and evolution against cancer. *Nature*
547 *Reviews Cancer* **14**, 371–380 (2014).
- 548 16. Hastings, A. *et al.* The spatial spread of invasions: new developments in theory and evidence.
549 *Ecology Letters* **8**, 91–101 (2005).
- 550 17. Jeschke, J. M. & Heger, T. *Invasion biology: hypotheses and evidence* (CABI, 2018).
- 551 18. Barton, N. H. & Charlesworth, B. Genetic revolutions, founder effects, and speciation. *Annual*
552 *review of ecology and systematics* **15**, 133–164 (1984).
- 553 19. Klopstein, S., Currat, M. & Excoffier, L. The fate of mutations surfing on the wave of a range
554 expansion. *Molecular biology and evolution* **23**, 482–490 (2006).
- 555 20. Hallatschek, O. & Nelson, D. R. Gene surfing in expanding populations. *Theoretical population*
556 *biology* **73**, 158–170 (2008).
- 557 21. Hallatschek, O. & Fisher, D. S. Acceleration of evolutionary spread by long-range dispersal.
558 *Proceedings of the National Academy of Sciences* **111**, E4911–E4919 (2014).
- 559

- 560 22. Kot, M., Lewis, M. A. & van den Driessche, P. Dispersal data and the spread of invading
561 organisms. *Ecology* **77**, 2027–2042 (1996).
- 562 23. Thomas, C. D. *et al.* Ecological and evolutionary processes at expanding range margins. *Nature*
563 **411**, 577–581 (2001).
- 564 24. Bénichou, O., Calvez, V., Meunier, N. & Voituriez, R. Front acceleration by dynamic selection
565 in Fisher population waves. *Physical Review E* **86**, 041908 (2012).
- 566 25. Shine, R., Brown, G. P. & Phillips, B. L. An evolutionary process that assembles phenotypes
567 through space rather than through time. *Proceedings of the National Academy of Sciences*
568 **108**, 5708–5711 (2011).
- 569 26. Van Ditmarsch, D. *et al.* Convergent evolution of hyperswarming leads to impaired biofilm
570 formation in pathogenic bacteria. *Cell reports* **4**, 697–708 (2013).
- 571 27. Korolev, K. S. The fate of cooperation during range expansions. *PLoS Comput Biol* **9**,
572 e1002994 (2013).
- 573 28. Yi, X. & Dean, A. M. Phenotypic plasticity as an adaptation to a functional trade-off. *Elife*
574 **5**, e19307 (2016).
- 575 29. Fraebel, D. T. *et al.* Environment determines evolutionary trajectory in a constrained pheno-
576 typic space. *Elife* **6**, e24669 (2017).
- 577 30. Ni, B. *et al.* Evolutionary remodeling of bacterial motility checkpoint control. *Cell reports* **18**,
578 866–877 (2017).
- 579 31. Shih, H.-Y., Mickalide, H., Fraebel, D. T., Goldenfeld, N. & Kuehn, S. Biophysical constraints
580 determine the selection of phenotypic fluctuations during directed evolution. *Physical biology*
581 **15**, 065003 (2018).
- 582 32. Deforet, M., Carmona-Fontaine, C., Korolev, K. S. & Xavier, J. B. Evolution at the edge of
583 expanding populations. *The American Naturalist* **194**, 291–305 (2019).
- 584 33. Phillips, B. L., Brown, G. P., Webb, J. K. & Shine, R. Invasion and the evolution of speed in
585 toads. *Nature* **439**, 803–803 (2006).
- 586 34. Travis, J. M. & Dytham, C. Dispersal evolution during invasions. *Evolutionary Ecology Re-
587 search* **4**, 1119–1129 (2002).
- 588 35. Taylor, C. M. & Hastings, A. Allee effects in biological invasions. *Ecology Letters* **8**, 895–908
589 (2005).
- 590 36. Korolev, K. S. Evolution arrests invasions of cooperative populations. *Physical review letters*
591 **115**, 208104 (2015).
- 592 37. Datta, M. S., Korolev, K. S., Cvijovic, I., Dudley, C. & Gore, J. Range expansion promotes co-
593 operation in an experimental microbial metapopulation. *Proceedings of the National Academy
594 of Sciences* **110**, 7354–7359 (2013).
- 595 38. Allen, B., Gore, J. & Nowak, M. A. Spatial dilemmas of diffusible public goods. *Elife* **2**, e01169
596 (2013).
- 597 39. Bauer, M. & Frey, E. Multiple scales in metapopulations of public goods producers. *Physical
598 Review E* **97**, 042307 (2018).
- 599 40. Stempler, O. *et al.* Interspecies nutrient extraction and toxin delivery between bacteria. *Nature
600 communications* **8**, 1–9 (2017).

- 601 41. Drancourt, M., Bollet, C., Carta, A. & Rousselier, P. Phylogenetic analyses of Klebsiella
602 species delineate Klebsiella and Raoultella gen. nov., with description of Raoultella ornithi-
603 nolytica comb. nov., Raoultella terrigena comb. nov. and Raoultella planticola comb. nov.
604 *International journal of systematic and evolutionary microbiology* **51**, 925–932 (2001).
- 605 42. Ershadi, A., Weiss, E., Verduzco, E., Chia, D. & Sadigh, M. Emerging pathogen: a case and
606 review of Raoultella planticola. *Infection* **42**, 1043–1046 (2014).
- 607 43. Simmons, A. D. & Thomas, C. D. Changes in dispersal during species' range expansions. *The*
608 *American Naturalist* **164**, 378–395 (2004).
- 609 44. Waters, J. M., Fraser, C. I. & Hewitt, G. M. Founder takes all: density-dependent processes
610 structure biodiversity. *Trends in ecology & evolution* **28**, 78–85 (2013).
- 611 45. Birzu, G., Matin, S., Hallatschek, O. & Korolev, K. S. Genetic drift in range expansions is
612 very sensitive to density dependence in dispersal and growth. *Ecology Letters* **22**, 1817–1827
613 (2019).
- 614 46. Excoffier, L., Foll, M. & Petit, R. J. Genetic consequences of range expansions. *Annual Review*
615 *of Ecology, Evolution, and Systematics* **40**, 481–501 (2009).
- 616 47. Roques, L., Garnier, J., Hamel, F. & Klein, E. K. Allee effect promotes diversity in traveling
617 waves of colonization. *Proceedings of the National Academy of Sciences* **109**, 8828–8833 (2012).
- 618 48. Slatkin, M. & Excoffier, L. Serial founder effects during range expansion: a spatial analog of
619 genetic drift. *Genetics* **191**, 171–181 (2012).
- 620 49. Bosshard, L. *et al.* Accumulation of deleterious mutations during bacterial range expansions.
621 *Genetics* **207**, 669–684 (2017).
- 622 50. Yan, J., Nadell, C. D., Stone, H. A., Wingreen, N. S. & Bassler, B. L. Extracellular-matrix-
623 mediated osmotic pressure drives *Vibrio cholerae* biofilm expansion and cheater exclusion.
624 *Nature communications* **8**, 1–11 (2017).
- 625 51. Xiong, L. *et al.* Flower-like patterns in multi-species bacterial colonies. *Elife* **9**, e48885 (2020).
- 626 52. Hallatschek, O., Hersen, P., Ramanathan, S. & Nelson, D. R. Genetic drift at expanding
627 frontiers promotes gene segregation. *Proceedings of the National Academy of Sciences* **104**,
628 19926–19930 (2007).
- 629 53. Korolev, K. S., Avlund, M., Hallatschek, O. & Nelson, D. R. Genetic demixing and evolution
630 in linear stepping stone models. *Reviews of modern physics* **82**, 1691 (2010).
- 631 54. Korolev, K. S. *et al.* Selective sweeps in growing microbial colonies. *Physical Biology* **9**, 026008
632 (2012).
- 633 55. Korolev, K. S., Xavier, J. B., Nelson, D. R. & Foster, K. R. A quantitative test of population
634 genetics using spatiogenetic patterns in bacterial colonies. *The American Naturalist* **178**, 538–
635 552 (2011).
- 636 56. Müller, M. J., Neugeboren, B. I., Nelson, D. R. & Murray, A. W. Genetic drift opposes mutu-
637 alism during spatial population expansion. *Proceedings of the National Academy of Sciences*
638 **111**, 1037–1042 (2014).
- 639 57. Momeni, B., Brileya, K. A., Fields, M. W. & Shou, W. Strong inter-population cooperation
640 leads to partner intermixing in microbial communities. *elife* **2**, e00230 (2013).
- 641 58. Prindle, A. *et al.* Ion channels enable electrical communication in bacterial communities.
642 *nature* **527**, 59–63 (2015).

- 643 59. Mitri, S., Clarke, E. & Foster, K. R. Resource limitation drives spatial organization in microbial
644 groups. *The ISME journal* **10**, 1471–1482 (2016).
- 645 60. Cremer, J. *et al.* Chemotaxis as a navigation strategy to boost range expansion. *Nature* **575**,
646 658–663 (2019).
- 647 61. Fisher, R. A. The wave of advance of advantageous genes. *Annals of eugenics* **7**, 355–369
648 (1937).
- 649 62. Kolmogorov, A. N. A study of the equation of diffusion with increase in the quantity of matter,
650 and its application to a biological problem. *Moscow University Bulletin of Mathematics* **1**, 1–
651 25 (1937).
- 652 63. Murray, J. D. *Mathematical Biology* (Berlin: Springer, 2003).
- 653 64. Birzu, G., Hallatschek, O. & Korolev, K. S. Fluctuations uncover a distinct class of traveling
654 waves. *Proceedings of the National Academy of Sciences* **115**, E3645–E3654 (2018).
- 655 65. Levin, D. A. & Kerster, H. W. The dependence of bee-mediated pollen and gene dispersal
656 upon plant density. *Evolution*, 560–571 (1969).
- 657 66. Courchamp, F., Clutton-Brock, T. & Grenfell, B. Inverse density dependence and the Allee
658 effect. *Trends in ecology & evolution* **14**, 405–410 (1999).
- 659 67. Matthysen, E. Density-dependent dispersal in birds and mammals. *Ecography* **28**, 403–416
660 (2005).
- 661 68. Kearns, D. B. A field guide to bacterial swarming motility. *Nature Reviews Microbiology* **8**,
662 634–644 (2010).
- 663 69. Peischl, S. & Gilbert, K. J. Evolution of dispersal can rescue populations from expansion load.
664 *The American Naturalist* **195**, 349–360 (2020).
- 665 70. Nadell, C. D., Foster, K. R. & Xavier, J. B. Emergence of spatial structure in cell groups and
666 the evolution of cooperation. *PLoS Comput Biol* **6**, e1000716 (2010).
- 667 71. Cremer, J. *et al.* Cooperation in microbial populations: theory and experimental model sys-
668 tems. *Journal of molecular biology* **431**, 4599–4644 (2019).
- 669 72. Tilman, D. Competition and biodiversity in spatially structured habitats. *Ecology* **75**, 2–16
670 (1994).
- 671 73. Bonte, D. *et al.* Costs of dispersal. *Biological reviews* **87**, 290–312 (2012).
- 672 74. Gude, S. *et al.* Bacterial coexistence driven by motility and spatial competition. *Nature* **578**,
673 588–592 (2020).
- 674 75. Farrell, F., Hallatschek, O., Marenduzzo, D. & Waclaw, B. Mechanically driven growth of
675 quasi-two-dimensional microbial colonies. *Physical review letters* **111**, 168101 (2013).
- 676 76. Warren, M. R. *et al.* Spatiotemporal establishment of dense bacterial colonies growing on hard
677 agar. *Elife* **8**, e41093 (2019).
- 678 77. Van Dyken, J. D., Müller, M. J., Mack, K. M. & Desai, M. M. Spatial population expansion
679 promotes the evolution of cooperation in an experimental prisoner’s dilemma. *Current Biology*
680 **23**, 919–923 (2013).
- 681 78. Kehe, J. *et al.* Massively parallel screening of synthetic microbial communities. *Proceedings of*
682 *the National Academy of Sciences* **116**, 12804–12809 (2019).

- 683 79. Schlechter, R. O. *et al.* Chromatic Bacteria – A Broad Host-Range Plasmid and Chromosomal
684 Insertion Toolbox for Fluorescent Protein Expression in Bacteria. *Frontiers in Microbiology*
685 **9**, 3052. ISSN: 1664-302X (2018).
- 686 80. Van der Walt, S. *et al.* scikit-image: image processing in Python. *PeerJ* **2**, e453. ISSN: 2167-
687 8359 (2014).
- 688 81. Press, W. H., Teukolsky, S. A., Vetterling, W. T. & Flannery, B. P. *Numerical recipes 3rd*
689 *edition: The art of scientific computing* (Cambridge university press, 2007).
- 690 82. Born, M. & Wolf, E. *Principles of optics: electromagnetic theory of propagation, interference*
691 *and diffraction of light* (Elsevier, 2013).